Changes in physico-chemical properties of iron-based Fischer–Tropsch catalyst induced by SiO_2 addition

H. Dlamini *, T. Motjope, G. Joorst, G. ter Stege, and M. Mdleleni *

Sasol Technology, 1 Klasie Havenga Avenue, Sasolburg 1947, South Africa

Received 18 May 2001; accepted 6 October 2001

The effect of adding SiO_2 to a precipitated Fe-based Fischer–Tropsch catalyst was investigated. Silica was added to the catalyst either during or after precipitation. The iron-based Fischer–Tropsch catalysts were studied using Mössbauer spectroscopy, BET surface area, XRD and SEM characterization methods. Adding SiO_2 to the catalyst during precipitation or immediately after precipitation (*i.e.*, precipitated SiO_2) results in the formation of Fe crystallites with an average diameter less than 3 nm, which have high surface areas and exhibit a strong interaction with the SiO_2 matrix. Consequently, these crystallites are resistant to reduction and carburisation. When SiO_2 was added to the catalyst after heat treatment (*i.e.*, binder SiO_2), the resulting catalyst was observed to consist of segregated SiO_2-rich and Fe-rich phases. The distribution of K_2O in both these phases indicates that the amount of effective K_2O, *i.e.*, that associated with Fe, is less when SiO_2 is added as a binder. The low extent of reduction and carburisation observed with catalysts that contain precipitated SiO_2 results in catalysts with low % CO conversion. A positive correlation between the amount of iron carbides present in the catalyst and the % CO conversion was observed in these studies.

KEY WORDS: iron catalyst; Fischer–Tropsch reaction

1. Introduction

The Fischer–Tropsch process involves the hydrogenation of CO in the presence of a catalyst, mainly Group VIIIA metals, to produce hydrocarbons and oxygenated compounds. The use of iron-based catalysts to catalyze this reaction dates as far back as the time of its discovery in 1923 [1]. Although more than 7 decades have passed from the first application of iron-based catalysts in the Fischer–Tropsch catalyst, there are still unabated attempts to understand and improve factors that affect the catalyst activity, selectivity and stability [2]. Most of these attempts have focused on the addition of "chemical promoters" such as K_2O and Cu [3–5] as well as "structural promoters" especially SiO_2, Al_2O_3 and TiO_2 [6,7]. "Chemical promoters" have always been thought to have an effect on the chemical behavior of iron catalysts such as facilitating the reduction of Fe_2O_3 to α-Fe as well as the adsorption and dissociation of CO. "Structural promoters" serve the purpose of stabilizing small iron oxide crystallites from sintering and providing the necessary mechanical integrity of the catalyst.

The distinction between chemical and structural promoters has faded in the past two decades. Bartholomew [6] reported that metal–support interactions in Ni-based catalysts affect the adsorption of CO and H_2 as well as the selectivity towards C_{2+} hydrocarbons. Egiebor [8] observed that changing the SiO_2 content of precipitated iron-based catalysts affects the branched hydrocarbons and internal olefin selectivities of the gasoline range products. The effect of adding different amounts of SiO_2 on the reducibility of these catalysts was however not mentioned in this paper. Jothimurugesan [9] reported that the amount of SiO_2 added to a precipitated 100 Fe/5 Cu/4.2 K catalyst influences the reducibility, attrition resistance and selectivity of the catalyst. Furthermore, addition of SiO_2 as a binder gave different results to those obtained when SiO_2 was precipitated with Fe, Cu and K [9]. Basu [10] reported that the addition of SiO_2 to precipitated iron catalysts decreases the catalyst activity. The discussion of the effect of the dilution of Fe due to the addition of SiO_2, crystallite size changes and different degrees of reduction on the catalyst performance is however lacking.

In this paper we report on the effect of adding SiO_2 during the preparation of a precipitated iron-based catalyst on (i) the catalyst phase composition during reduction and at the end of a Fischer–Tropsch (FT) synthesis run, (ii) extent of reduction, (iii) surface area and (iv) catalytic performance. Mössbauer spectroscopy was used extensively, in an attempt to correlate catalytic behavior with the catalyst phase composition and extent of reduction.

2. Experimental

2.1. Catalyst preparation

The Fe, Cu, K salts and NH_4OH solution used in this study were purchased from C.J. Labs and were used as received. The iron-based catalysts used in this study were prepared *via* a continuous precipitation procedure, which is similar to the one described by Diffenbach [11], using reagent

* To whom correspondence should be addressed. E-mail: {Humphrey.Dlamini; Millan.Mdleleni}@sasol.com

1011-372X/02/0300-0201/0

Table 1
Details of the catalysts used in this study

Catalyst	Composition/100 g Fe	SiO_2 addition
BC1	4.7 g Cu/0.2 g K_2O/21.5 g SiO_2	To the metal salt solution prior to precipitation
BC2	5.1 g Cu/0.2 g K_2O/19.5 g SiO_2	After precipitation
BC3	4.9 g Cu/0.2 g K_2O/23.7 g SiO_2	After drying at 397 K
BC4	5.2 g Cu/0.2 g K_2O/25.5 g SiO_2	After calcination at 723 K
BC12	4.4 g Cu/0.2 g K_2O/0 g SiO_2	No SiO_2 added

grade ammonium hydroxide as a precipitating agent. Precipitation was performed at 71 °C, the flow rates of the two solutions were adjusted to give a constant pH of ∼8 at mixing. A sol consisting of 41% (w/w) SiO_2 was added at different stages during catalyst preparation. Immediately after precipitation the precipitates were centrifuged for 2 min at 8000 rpm and then separated from the supernatant without aging or washing. The catalysts were dried at 393 K for 24 h and then calcined in air at 673 K for 5 h. Details of the stages at which SiO_2 was added and the elemental analysis data of these catalysts are presented in table 1. SiO_2 added to BC 1 and 2 will be referred to as precipitated SiO_2 and that added to BC 3 and 4 as binder SiO_2.

2.2. Catalyst characterization

Mössbauer spectroscopy experiments were performed on fresh, reduced and spent catalysts using a 50 mCi Co-57 source in a rhodium matrix. The spectrometer was operated in the symmetric constant acceleration mode with 100 us of dwell time per channel. The spectra were collected over 1024 channels in mirror image format. Data analysis was performed using a least-squares fitting routine that models the spectra as a combination of singlets, quadruple doublets and magnetic sextuplets based on a Lorenzian line shape profile. Identification of the spectral components was based on the comparison of their isomeric shift (δ), quadruple splitting (Δ) and hyperfine magnetic field (H) values with those reported in the literature, such as MERDJ. All isomer shift and magnetic hyperfine field values are reported relative to metallic iron (α-Fe). Quantification of the various spectral components is based on the assumption that the different iron containing species have similar recoil free fractions (f_1).

XRD experiments on fresh samples were performed with a Siemens SD500 diffractometer with Fe-filtered Co Kα radiation as a primary X-ray beam. Information about crystallite size was obtained by applying the Scherrer equation [12] to the most intense peak of the X-ray pattern taking into account that this equation is only applicable for crystallites with mean diameters between 3 and 50 nm [13]. A value of 0.9 was used for the Scherrer constant (K) and the line width was expressed in terms of Δ (2θ) (radians).

Scanning electron microscopy (SEM) measurements were performed using a model 1430 LEO SEM fitted with a tungsten filament and operated at 25 kV. An integrated iXRF energy dispersive X-ray spectrometer (EDS) was employed to obtain quantitative information on the distribution of Si, K, Fe and Cu atoms. The samples were prepared by setting the powder-like precipitated iron catalysts in a resin (EPOFIX). The set samples were polished in order to obtain smooth cross-sections of relevant areas of the catalyst. The polished surfaces were sputter coated with gold/palladium for 80 s in 20 s intervals.

The total surface area data was obtained *via* N_2 adsorption at liquid nitrogen temperature with a Micromeritics Gemini surface area analyzer using the BET method. This technique also allows for the determination of total pore volume.

2.3. Catalyst evaluation

Catalysts were reduced *ex situ* in a flow of UHP H_2, supplied by Fedgas, at 513 K for 16 h; 1 bar and a GHSV of $1\,l\,g^{-1}\,h^{-1}$ in an all glass reactor. The reduced samples were passivated in molten wax, to mitigate catalyst re-oxidation, prior to MES analyses.

FT synthesis experiments were performed in a fixed-bed reactor with sieved fractions of catalyst between 38 and 150 μm. The catalysts were reduced *in situ* (20 bar, 513 K, 16 h, GHSV of $1\,l\,g^{-1}\,h^{-1}$) and then treated with synthesis gas ($H_2/CO = 2$) at 20 bar, 513 K and a GHSV of $3\,l\,g^{-1}\,h^{-1}$. The FT experiments were performed over a period of 100–150 h. Gas samples were periodically extracted from the reactor inlet and exit for analyses with a gas chromatograph.

3. Results and discussion

3.1. Characterisation

3.1.1. Fresh samples

The surface areas of the catalysts after calcination are presented in table 2. Although these catalysts contain the same amounts of metal components and SiO_2, these data show

Table 2
Physical properties of catalysts

Catalyst	Surface area ($m^2\,g^{-1}$)	Total pore volume ($cm^3\,g^{-1}$)	Average crystallite size[a] (nm)
BC1	198	0.36	>3
BC2	185	0.31	>3
BC3	176	0.43	5
BC4	107	0.21	7
BC12	88	0.14	9

[a] Determined *via* XRD analyses for both iron phases present in the sample.

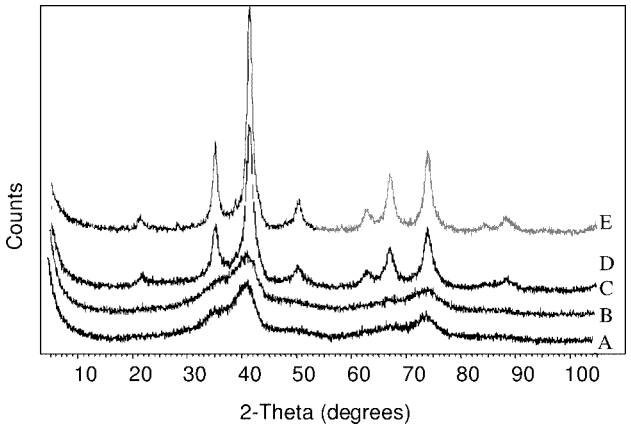

Figure 1. XRD patterns of fresh samples: (A) BC1, (B) BC2, (C) BC3, (D) BC4, (E) BC12.

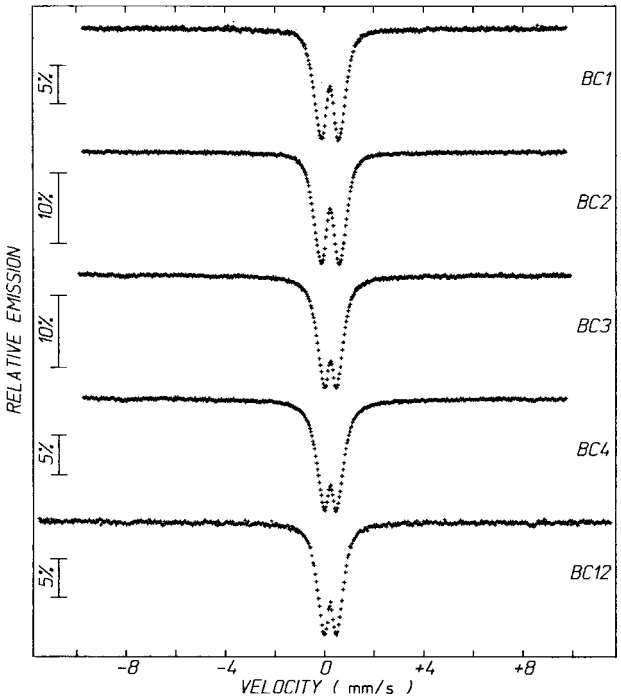

Figure 2. MES spectra of fresh samples.

that the stage at which SiO_2 is added during the preparation of precipitated iron-based catalysts has an effect on the surface area of the final product. Adding SiO_2 during the initial stage of the precipitation process results in a catalyst with the highest surface area (BC1).

The XRD patterns of the as-prepared catalysts are presented in figure 1 and these revealed the presence of $Fe(OH)_3$ and a spinel phase, $CuFe_2O_4$. The crystallite size and amount of both these phases varies with the stage at which SiO_2 was added. Catalysts where SiO_2 was added during the initial stages of precipitation have small crystallites of $Fe(OH)_3$, whereas the catalysts where SiO_2 was added before drying or after calcination consist of larger crystallites of $Fe(OH)_3$ and $CuFe_2O_4$. This observation in combination with the surface area data indicates that the presence of SiO_2, especially when added before any thermal treatment, hinders the sintering of small crystallites of $Fe(OH)_3$ and $CuFe_2O_4$.

The phase composition determined from XRD data was validated by MES analyses. The MES spectra of fresh samples are presented in figure 2 and the hyperfine interaction parameters obtained from the analyses of these spectra are presented in table 3. An indication about the average crystallite size was obtained from [14]:

$$d_{\mathrm{p}} = \frac{0.9}{D}, \tag{1}$$

where d_{p} is the average crystallite diameter in nm and D is the ratio of the spectral area corresponding to atoms located on the "surface" to those located in the "bulk" of the crystallites. Consistent with the XRD data discussed above MES analyses of the catalysts reveal that precipitated SiO_2 results in the formation of smaller crystallites of Fe^{3+}-containing species than binder SiO_2. The different quadruple splitting values obtained between different samples are most probably an indication of different extents of metal–support interaction.

Backscatter images and X-ray elemental maps obtained from scanning electron microscopy analyses are presented in figure 3 (a), (b) and (c). These images indicate that the distribution of SiO_2 in the catalysts is affected by the manner in which SiO_2 is added to the catalyst. SEM micrographs of catalysts where SiO_2 was added immediately after drying or after calcination (*i.e.*, binder SiO_2) reveal an uneven distribution of SiO_2. The addition of an aqueous solution of SiO_2 resulted in the dissolution and migration of the basic promoter, K_2O. This is evident from the association of K_2O with both Fe-rich and SiO_2-rich regions. The implications for this are that the amount of effective K_2O, *i.e.*, directly associated with Fe, is reduced by the addition of SiO_2 as a binder. The distribution of other promoters such as Cu is not affected. X-ray elemental maps of catalysts that contain precipitated SiO_2 show an even distribution of promoters as expected.

Table 3
Hyperfine interaction parameters obtained from MES spectra of the fresh sample

Sample	IS_{Fe} ($mm\,s^{-1}$)	QS ($mm\,s^{-1}$)	Phase	Relative average crystallite size
BC1	0.34	1.12	Fe^{3+}	1
	0.35	0.63	Fe^{3+}	
BC2	0.34	1.08	Fe^{3+}	1.13
	0.35	0.61	Fe^{3+}	
BC3	0.34	0.83	Fe^{3+}	1.18
	0.35	0.44	Fe^{3+}	
BC4	0.34	0.98	Fe^{3+}	1.23
	0.34	0.45	Fe^{3+}	
BC12	0.33	0.86	Fe^{3+}	1.33
	0.33	0.47	Fe^{3+}	

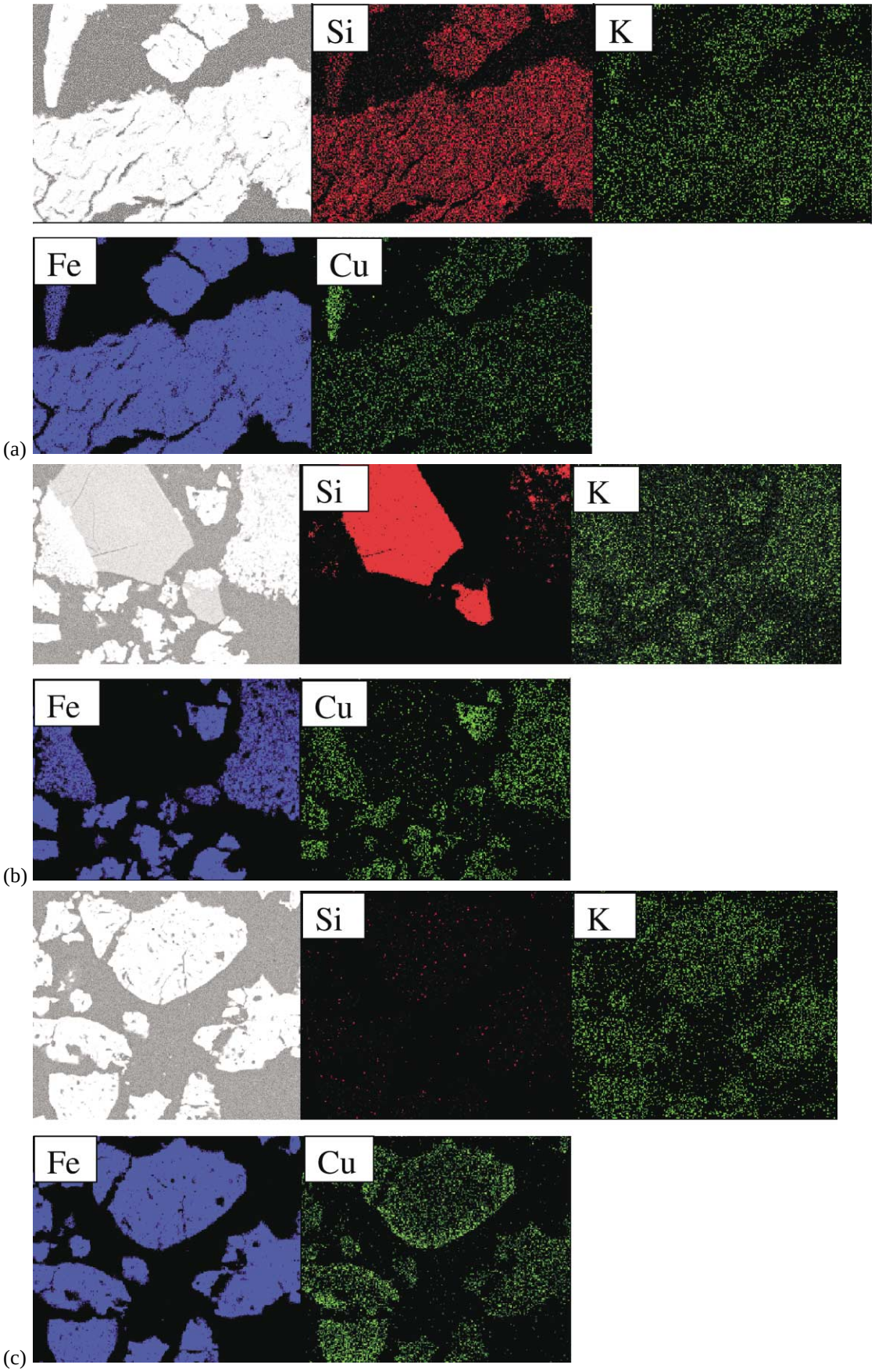

Figure 3. (a) SEM micrograph and X-ray maps of BC1, showing the distribution of elements. (b) SEM micrograph and X-ray maps of BC4, showing the distribution of elements. (c) SEM micrograph and X-ray maps of BC12, showing the distribution of promoters.

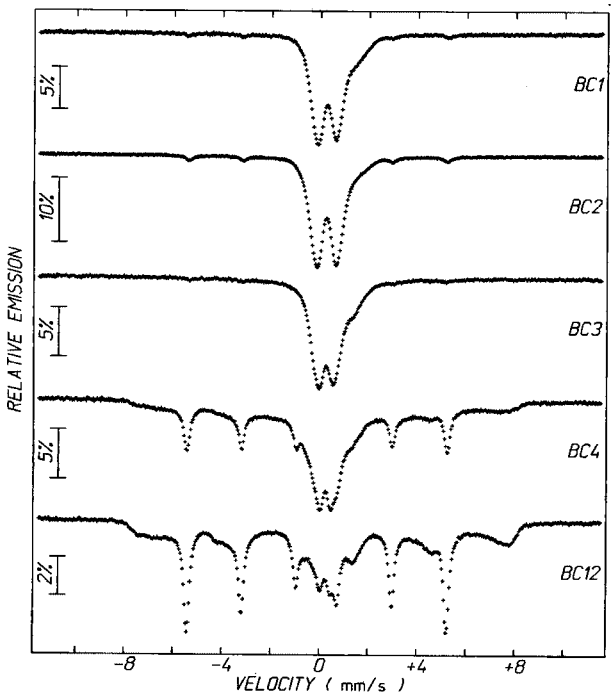

Figure 4. MES spectra of samples following reduction in H_2.

Table 4
Hyperfine interaction parameters following reduction in H_2

Sample	IS_{Fe} ($mm\,s^{-1}$)	QS ($mm\,s^{-1}$)	B_{HF} (T)	Phase
BC2	0.02	0.00	32.8	α-Fe
	0.36	0.89	–	Fe^{3+}
	0.88	1.57	–	Fe^{2+}
	0.02	0.00	32.9	α-Fe
BC1	0.35	0.84	–	Fe^{3+}
	0.89	1.36	–	Fe^{2+}
BC3	0.02	0.00	32.8	α-Fe
	0.36	0.73	–	Fe^{3+}
	0.88	1.24	–	Fe^{2+}
BC4	0.00	0.00	33.1	α-Fe
	0.26	−0.03	47.1	Fe_3O_4
	0.66	0.08	43.1	
	0.35	0.62	–	Fe^{3+}
	0.99	1.13	–	Fe^{2+}
BC12	0.00	0.00	33.0	α-Fe
	0.04	0.00	–	α-Fe
	0.26	0.04	47.1	Fe_3O_4
	0.45	0.05	43.1	
	0.35	0.50	–	Fe^{3+}
	1.11	0.90	–	Fe^{2+}

3.1.2. Reduced samples

Figure 4 presents MES spectra of catalysts following reduction in H_2. Hyperfine interaction parameters obtained from the analyses of these spectra are presented in table 4. The amounts of the various phases present in the catalyst after reduction are presented in figure 5. These data indicate that a homogeneous distribution of Fe in the SiO_2 matrix hinders the reduction Fe^{3+} to Fe^0. Catalysts where SiO_2 was added before or after precipitation as well as the one where SiO_2 was added after drying consist of more than 75% Fe^{3+}, minute amounts (<6%) of α-Fe and the remainder of iron exists as Fe^{2+}. This Fe^{2+} species seems to be stabilized by an intimate interaction of iron with SiO_2 (*cf.* BC1, BC2, BC3 with BC4, figure 3 *vide supra*). Comparison of BC3 and BC4 shows that the extent of reduction of these SiO_2 bound catalysts is dependent on the treatment of the catalyst prior to binding with SiO_2. Catalysts calcined prior to binding with SiO_2 are relatively easy to reduce, an observation attributed to reduced interaction of the metal oxide and SiO_2.

Previous studies by Jothimurugesan [9] and Bukur [15] have proposed that the amount of SiO_2 added to an iron-based catalyst affects the extent of reduction. However, the data presented herein reveals that the extent of reduction of SiO_2 promoted iron catalysts is also dependent on the manner in which SiO_2 is added to the catalyst as this affects the distribution of Fe in the SiO_2 matrix. Furthermore, an intimate interaction of SiO_2 with iron hinders the formation of large crystallites of Fe_3O_4, whilst stabilizing superparamagnetic Fe^{2+}-containing species.

3.1.3. Spent samples

The phase compositions and MES spectra of samples following Fischer–Tropsch synthesis are presented in figures 6 and 7, respectively. Hyperfine interaction parameters ob-

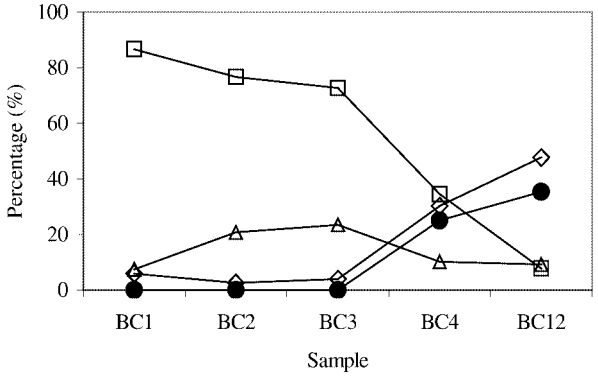

Figure 5. Catalyst phase composition following reduction: (◊) Fe, (□) Fe^{3+}, (△) Fe^{2+} and (•) Fe_3O_4.

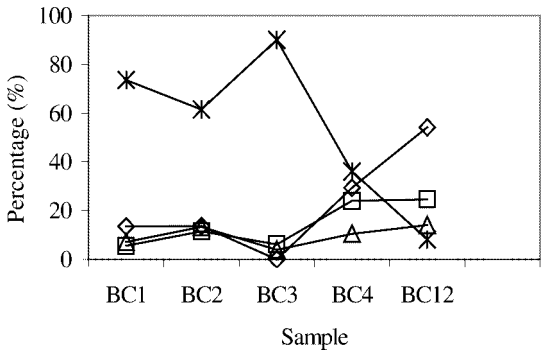

Figure 6. Phase composition of samples following Fischer–Tropsch synthesis: (◊) Fe2.5C, (□) Fe2.2C, (△) Fe^{2+} and (∗) Fe^{3+}.

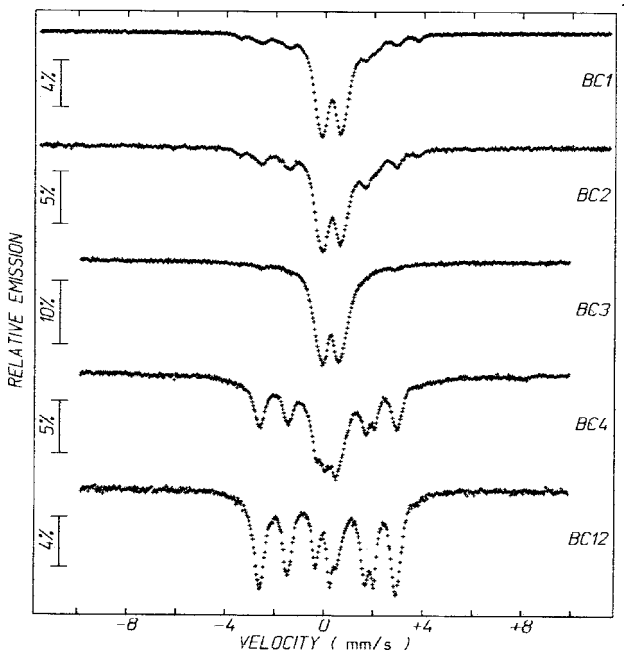

Figure 7. MES spectra of samples following Fischer–Tropsch synthesis.

tained from an analysis of these spectra are presented in table 5. The amount of Fe^{3+} present in these catalysts decreases on moving from BC12 to BC1, except for BC3, which shows less reduction and consequently less carbide formation. The anomalous behavior observed with BC3 warrants further investigation. It can be inferred from the data that α-Fe, Fe_3O_4 and Fe^{2+} that were formed during reduction are converted to a mixture of χ-$Fe_{2.5}C$ and ε'-$Fe_{2.2}C$, except for BC3, which shows ε'-$Fe_{2.2}C$ as the only carbide during Fischer–Tropsch synthesis.

Table 5
Hyperfine interaction parameters of catalysts after Fischer–Tropsch synthesis

Sample ID	IS_{Fe} ($mm\,s^{-1}$)	QS ($mm\,s^{-1}$)	B_{HF} (T)	Phase
BC1	0.25	0.06	22.3	χ-$Fe_{2.5}C$
	0.18	0.11	17.7	
	0.27	0.07	10.1	ε'-$Fe_{2.2C}$
	0.20	0.11	16.4	
	0.88	2.16	–	Fe^{2+}
	0.38	0.81	–	Fe^{3+}
BC2	0.26	0.07	22.3	χ-$Fe_{2.5}C$
	0.22	0.08	18.3	
	0.20	0.15	11.1	ε'-$Fe_{2.2C}$
	0.22	0.06	16.6	
	0.88	1.91	–	Fe^{2+}
	0.40	0.79	–	Fe^{3+}
BC3	0.24	0.16	16.9	ε'-$Fe_{2.2}C$
	1.02	1.61	–	Fe^{2+}
	0.36	0.79	–	Fe^{3+}
BC4	0.20	0.11	22.7	χ-$Fe_{2.5}C$
	0.20	0.08	17.9	
	0.21	0.17	11.1	ε'-$Fe_{2.2C}$
	0.23	0.07	16.5	
	1.21	1.83	–	Fe^{2+}
	0.39	0.76	–	Fe^{3+}
BC12	0.20	0.17	11.0	χ-$Fe_{2.5}C$
	0.24	0.06	17.5	
	0.27	0.17	22.0	
	0.25	0.06	16.3	ε'-$Fe_{2.2}C$
	1.24	1.78	–	Fe^{2+}
	0.35	1.06	–	Fe^{3+}

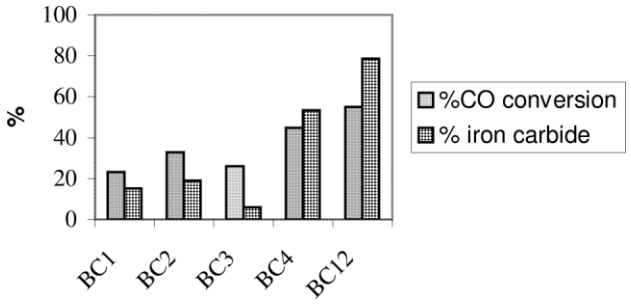

Figure 8. Variation of % CO conversion and iron carbide as a function of the stage at which SiO_2 was added.

The degree of carburisation is dependent on the stage at which SiO_2 was added. Addition of SiO_2 during or after precipitation leads to catalysts containing less carbidic iron species compared to those where SiO_2 was added as binder, BC4. Comparison of data obtained for BC1 and BC2 reveals that adding SiO_2 during precipitation induces a stronger metal–support interaction than when SiO_2 is added after precipitation.

3.2. Kinetic experiments

Preliminary results obtained during Fischer–Tropsch synthesis are presented in figure 8. These catalysts are compared under steady state conditions, which is often reached within the first 20 h with Fe-based catalysts. Except for BC3, the % CO conversion for catalysts that have an even distribution of SiO_2 is lower than that for catalysts where SiO_2 is sparsely associated with the active metal. Although SEM analysis of BC1 and BC2 indicated an almost similar distribution of SiO_2, these catalysts exhibit different catalytic behavior. The former is less active than the latter. The observed differences in catalytic behavior can be attributed to the relatively stronger metal–support interactions in the former than the latter, consistent with earlier discussions. Furthermore, there is evidence of a positive correlation between the catalyst activity and the amount of carbidic iron species formed during Fischer–Tropsch synthesis.

4. Conclusions

The stage at which SiO_2 is added during the preparation of precipitated iron-based catalysts determines the catalyst properties such as the crystallite size of the active component, surface area, total pore volume and reduction behav-

ior as well as the activity during Fischer–Tropsch synthesis. Precipitated SiO_2, *i.e.*, SiO_2 added before or just after precipitation, results in catalysts with high surface area; however this induces a strong interaction between the active metal and SiO_2 due to an intimate mixing of the two components. Furthermore, this interaction hinders the reduction and carburisation of iron-containing crystallites. The low degree of reduction and extent of carbidic iron formation causes the activity of catalysts prepared in this manner to be relatively low. These effects appear to be more pronounced for catalysts where SiO_2 was added before precipitation, *i.e.*, to the metal salt solution.

Adding SiO_2 as a binder, *i.e.*, after thermal treatment, such as drying or calcination, results in catalysts with lower surface area, enhanced phase segregation between SiO_2 and the active components, and consequently higher degrees of reduction. These effects were more pronounced when SiO_2 was added after calcination. There is evidence that the catalyst where SiO_2 is added after drying is re-oxidized during Fischer–Tropsch synthesis. This catalyst had the lowest amount of iron carbides as well as % CO conversion during Fischer–Tropsch synthesis.

Optimal catalytic behavior that corresponded with a maximum amount of iron carbides was observed with the catalyst that does not contain SiO_2. However this catalyst might not have the required strength for application in fluidized and slurry bed reactors. In general, the activity of these catalysts correlates well with the amount of iron carbides formed during Fischer–Tropsch synthesis. This observation supports prior studies in several laboratories [2,16,17] that iron carbides are the primary active species during Fischer–Tropsch synthesis with iron-based catalysts.

Acknowledgment

The authors wish to thank Sasol Technology for providing the resources to perform this research, Mrs. B. Breedt, Mr. L. Wedemeyer, Mrs. E. du Plessis and Dr. H. Retief for performing surface characterisation and XRD experiments.

References

[1] F. Fischer and H. Tropsch, Brennstoff-Chem. 8 (1927).
[2] A.K. Datye, J. Yaming, L. Mansker, T. Motjope, T.H. Dlamini and N.J. Coville, Stud. Surf. Sci. Catal. 130 (2000).
[3] M.E. Dry, in: *Catalysis Science and Technology*, Vol. 1, eds. R.B. Anderson and M. Bourdart (1981).
[4] E.S. Lox, G.B. Marin and E. de Grave, Appl. Catal. 40 (1988).
[5] D. Bukur, D. Mukesh and S. Patel, Ind. Eng. Chem. Res. 29 (1990).
[6] C. Bartholomew, R.B. Pannell and J.L. Butler, J. Catal. 65 (1980).
[7] G.C. Bond, in: *Metal–Support and Metal–Additive Effects in Catalysis*, ed. B. Imelik (1982).
[8] N.O. Egiebor and W.C. Cooper, Canad. J. Chem. Eng. 63 (1985).
[9] K. Jothimurugesan, J.J. Spivey, S.K. Gangwal and J.G. Goodwin, Jr., Stud. Surf. Sci. Catal. 119 (1998).
[10] P.K. Basu, S.B. Basu, S.K. Mitra, Y.C. Dasandhi, S.S. Bhattacherjee and P. Samuel, Stud. Surf. Sci. Catal. 113 (1998).
[11] R.A. Diffenbach and D.J. Fauth, J. Catal. 106 (1986).
[12] H.P. Klug and L.E. Alexander, *X-ray Diffraction Procedures for Polycrystalline and Amorphous Materials* (Wiley, New York, 1974).
[13] J.R. Anderson, *Structure of Metallic Catalysts* (Academic Press, London, 1975).
[14] E.S. Lox, G.B. Marin, E. de Grave and P. Brussière, Appl. Catal. 40 (1988).
[15] D.B. Bukur, X. Lang, D. Mukesh, W.H. Zimmerman, M.P. Rosynek and C. Li, Ind. Eng. Chem. Res. 29 (1990).
[16] G.B. Raupp and W.N. Delgass, J. Catal. 58 (1979).
[17] J.W. Niemantsverdriet, A.M. van der Kraan, W.L. van Dijk and H.S. van der Baan, J. Phys. Chem. 84 (1980).